

Concentrated solutions of single-chain nanoparticles: A simple model for intrinsically disordered proteins under crowding conditions

Angel J. Moreno,^{*,†,‡} Federica Lo Verso,[‡] Arantxa Arbe,[†] José A. Pomposo,^{†,¶,§}
and Juan Colmenero^{†,‡,¶}

*Centro de Física de Materiales (CSIC, UPV/EHU) and Materials Physics Center MPC,
Paseo Manuel de Lardizabal 5, 20018 San Sebastián, Spain , Donostia International
Physics Center (DIPC), Paseo Manuel de Lardizabal 4, 20018 San Sebastián, Spain ,
Departamento de Física de Materiales, Universidad del País Vasco (UPV/EHU), Apartado
1072, E-20800 San Sebastián, Spain, and IKERBASQUE - Basque Foundation for Science,
Alameda Urquijo 36, E-48011 Bilbao, Spain*

E-mail: wabmosea@ehu.es

*To whom correspondence should be addressed

[†]Centro de Física de Materiales (CSIC, UPV/EHU) and Materials Physics Center MPC, Paseo Manuel de Lardizabal 5, 20018 San Sebastián, Spain

[‡]Donostia International Physics Center (DIPC), Paseo Manuel de Lardizabal 4, 20018 San Sebastián, Spain

[¶]Departamento de Física de Materiales, Universidad del País Vasco (UPV/EHU), Apartado 1072, E-20800 San Sebastián, Spain

[§]IKERBASQUE - Basque Foundation for Science, Alameda Urquijo 36, E-48011 Bilbao, Spain

Abstract

By means of large-scale computer simulations and small-angle neutron scattering (SANS), we investigate solutions of single-chain nanoparticles (SCNPs), covering the whole concentration range from infinite dilution to melt density. The analysis of the conformational properties of the SCNPs reveals that these synthetic nano-objects share basic ingredients with intrinsically disordered proteins (IDPs), as topological polydispersity, generally sparse conformations, and locally compact domains. We investigate the role of the architecture of the SCNPs in their collapse behavior under macromolecular crowding. Unlike in the case of linear macromolecules, which experience the usual transition from self-avoiding to Gaussian random-walk conformations, crowding leads to collapsed conformations of SCNPs resembling those of crumpled globules. This behavior is already found at volume fractions (about 30 %) that are characteristic of crowding in cellular environments. The simulation results are confirmed by the SANS experiments. Our results for SCNPs — a model system free of specific interactions — propose a general scenario for the effect of steric crowding on IDPs: collapse from sparse conformations at high dilution to crumpled globular conformations in cell environments.

The compaction of individual polymer chains via single chain technology provides versatile ultra-small soft nano-objects (5-20 nm), the so-called single-chain nanoparticles (SCNPs).¹⁻⁴ Significant effort has been devoted in recent years to endow SCNPs with useful functions for nanomedicine,^{5,6} biosensing,⁷ bioimaging^{8,9} and catalysis applications.¹⁰⁻¹² Recent investigations by small-angle neutron and X-ray scattering (SANS and SAXS) have shed light on the conformational properties of the resulting SCNPs in solution.^{6,11,13,14} These works have revealed that, in general, SCNPs synthesized by means of state-of-the-art intrachain folding/collapse techniques show sparse, nonglobular conformations in dilute conditions.¹⁵ Computer simulations have elucidated the underlying physical mechanism for such sparse morphologies.¹⁴ In brief, the extended self-avoiding conformations of the linear precursor chains, in the good solvent conditions of synthesis, favour bonding of functional reactive

groups that are separated by short contour distances. This mechanism promotes local globulation along the chain, but is not efficient for global, large-scale chain compaction.^{14,15} The particular topology of the SCNPs has interesting consequences on their scaling properties. Thus, the size R of SCNPs *in good solvent and high dilution* scales with their molecular weight M as $R \sim M^\nu$, with an average exponent $\nu \approx 0.5$ (see compilation of literature data in Ref.¹⁵). This observation is rather different from the limits of self-avoiding linear chains¹⁶ (Flory exponent $\nu = 0.59$) and globular spherical objects ($\nu = 1/3$). Interestingly, the scaling behavior $\nu \approx 0.5$ generally found for SCNPs in good solvent is similar to that of linear chains *in θ -solvent*.¹⁶ Indeed there are some analogies between the structure of SCNPs and θ -chains, both having locally compact regions in globally sparse conformations.

The former scaling properties of SCNPs are also strikingly similar to those of intrinsically disordered proteins (IDPs) in dilute conditions, both having an average scaling exponent $\nu \approx 0.5$.¹⁷⁻¹⁹ This behavior is rather different from that of denatured unfolded and globular folded proteins, whose size scales with the number of residues in a similar fashion to self-avoiding linear and globular collapsed polymers, respectively. In general, IDPs are not fully disordered linear chains. Most of them have some degree of secondary structure. As a consequence IDPs are topologically polydisperse: different IDPs can show very different degrees of disorder and compactness.²⁰⁻²² Though secondary structure is absent in current SCNPs, we can still establish important analogies between the internal structure of IDPs and SCNPs: i) SCNPs are also topologically polydisperse;¹⁴ ii) as discussed below, both IDPs and SCNPs are characterized by the presence of locally compact, weakly deformable regions (domains) of the polypeptide/polymer chain connected by flexible disordered segments.

IDPs are highly abundant in eukaryotes.²¹ The biological function of IDPs is founded on their internal dynamics and flexibility, enabling them to respond quickly to environmental changes and to bind with different cellular targets. It was early realized that, as a direct consequence of their malleability, the structural, dynamic and associative properties of IDPs could be affected by macromolecular crowding *in vivo*, substantially differing

from the observations *in vitro* at highly dilute conditions. Indeed, in living cells the volume fraction occupied by biomacromolecules typically ranges from 10% to 40 %.²³ Beyond the role played by eventual specific interactions with the crowders, the excluded-volume effects created by such a reduction of the available space can have, by themselves, decisive effects on the function of IDPs.

A rapidly growing body of research has been devoted to the effect of macromolecular crowding on the physical properties of IDPs. Because of the complexity of the cell environment and the interplay between intervening factors (concentration, specific interactions, internal structure of the IDP...) the effect of crowding is highly variable between different IDPs, from playing a minor role to provoking dramatic changes with respect to dilute conditions.^{23–26} In order to investigate separately the effect of purely steric interactions, a series of experimental and simulation works have been performed in simple model systems of IDPs and crowders.^{27–30} Namely, linear polymers and big inert molecules have been used to mimick the IDPs and crowders, respectively. Very recently, Kang *et al.* have presented a detailed investigation on the size of a linear polymer chain in a concentrated solution of colloidal spherical crowders.³⁰ By using the crowder concentration and the size ratio λ between the polymer and the crowder as control parameters, they have proposed a general picture for the collapse of biopolymers under steric crowding. Thus, for long biopolymers as DNA (large λ) even weak crowding can lead to a coil-to-globule transition. This behavior is however not possible for much shorter molecules as IDPs ($\sim O(100)$ residues) even in the limit of close packing.³⁰

Though the former investigations on crowding effects on linear chains are important highlights in our understanding of properties of IDPs *in vivo*, they miss a general structural ingredient of IDPs. Namely, except in the limit of fully disordered IDPs, the linear topology is a too simplified representation of their intramolecular conformations. As aforementioned, IDPs generally contain some compact (ordered) regions or *domains* connected by flexible segments. The topological contribution of these regions to the interaction with the crowders

is fundamentally different from that of linear segments, and may result in very different collapse features for IDPs. With this idea in mind, in this Letter we aim to provide a general framework for the role of the steric crowding effects on IDP conformations in cell environments. We exploit structural analogies between SCNPs and IDPs and investigate conformational properties of SCNPs in concentrated solutions. Noting that this question has been essentially unexplored in the literature, the scope of our work is not limited to SCNPs but also has important consequences for collapse of IDPs under crowding. Thus, SCNPs provide a model system that shares universal structural features with IDPs —topological polydispersity, global flexibility, global sparse conformations and presence of locally compact domains— and is free of specific interactions, allowing to investigate separately the purely steric, excluded-volume contributions to crowding.

For this purpose, we combine large-scale simulations of a generic bead-spring model for solutions of SCNPs, and SANS experiments on real systems, covering the whole concentration range from infinite dilution to melt density. We analyze the role of the internal degree of disorder of the SCNP on its collapse behavior under macromolecular crowding. Our results for SCNPs propose a general scenario for IDPs: steric crowding in cell environments generally lead IDPs to adopt conformations resembling those of crumpled globular objects.^{31–33} The usual transition from self-avoiding to pure random-walk (Gaussian) conformations found for linear macromolecules¹⁶ is only a particular case, taking place in the limit of fully disordered IDPs.

We have simulated a simple bead-spring model of the SCNPs¹⁴ in good solvent conditions, see Supporting Information (SI) for details. A total of 200 SCNPs have been generated by irreversible intramolecular cross-linking of linear chains (*precursors*) with the same number of monomers ($N = 200$) and functional reactive groups (40%). An inspection of configurations reveals that in general SCNPs adopt sparse topologies, with locally compact regions (see Figure 1). In order to characterize such regions we introduce the concept of SCNP domains. To identify the domains, we proceed as follows:

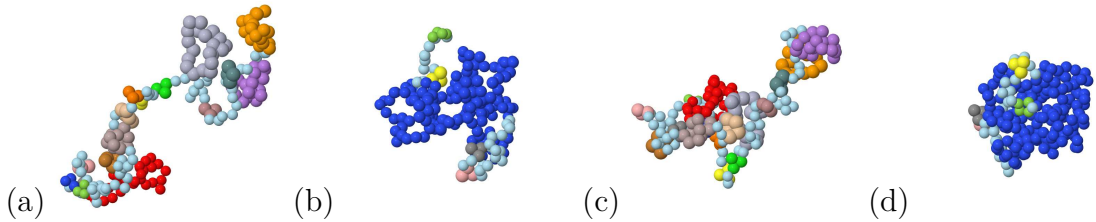


Figure 1: Panels (a) and (b): Snapshots of two selected SCNPs at infinite dilution ($\rho \rightarrow 0$). The SCNPs belong to the 10% with the lowest n_d^{\max} (a) and to the 10% with the lowest asphericity (b); see text for definitions. Panels (c) and (d): snapshots at $\rho = 0.4$ for the same SCNPs of panels (a) and (b), respectively. In all snapshots different domains are depicted in different colors. Monomers not belonging to a domain are depicted in light blue.

- i) We first identify *rings* in the cross-linked SCNP. Thus, if the functional monomers i_1 and $i_2 > i_1$ are bonded to each other, all the monomers $i_1 \leq i \leq i_2$ form a ring.
- ii) We establish that two rings belong to a same domain if they are mutually linked, i.e., if there are monomers belonging to both rings.
- iii) A ring is assigned to a domain if it is linked to at least one of the other rings contained in that domain. A ring that is not linked to any other ring is considered a (single-ring) domain.
- iv) Two domains merge into a single one if they have at least one ring in common.

Thus, a domain is a cluster of rings, where the criterion for clustering is having monomers in common. The procedure of steps i)-iv) provides an unambiguous, well-defined criterion for identifying domains based on the permanent connectivity structure of the SCNP. We find that some monomers do not belong to any domain. Thus, such monomers form flexible segments connecting domains. In average, 82 % of the monomers belong to some domain, though this fraction varies between different SCNPs in the range of 50% to 100 %, as a consequence of their topological polydispersity. Panels (a) and (b) of Figure 1 show snapshots of a sparse and a compact SCNP at infinite dilution ($\rho \rightarrow 0$, with ρ the density of monomers in the solution, see SI). Panels (c) and (d) show the same SCNPs in a concentrated solution (see discussion below). In Figure 1 the different domains, determined according to the procedure above, are depicted in different colors. The monomers connecting the different domains are

depicted in light blue. As can be seen in Figure 1, the domain size can largely vary from a few monomers to essentially the whole SCNP. Figure 2a shows the distribution, obtained from all the simulated SCNPs, of the domain size, this being defined by its number of monomers n_d . As anticipated by inspection of the snapshots, a broad distribution is found, covering the whole range of possible values, from the minimum single-ring domain ($n_d = 3$) to the whole SCNP ($n_d = N = 200$). Most of the domains are small: 55 % of them have $n_d \leq 6$ monomers, and even 44 % have the minimum size $n_d = 3$. This is a consequence of the self-avoiding character of the linear precursor in good solvent conditions, which strongly promotes bonding of functional monomers separated by short contour distances. This mechanism leads to the formation of a large fraction of small rings that do not even share monomers with others (i.e., single-ring domains). However, there is also a significant fraction of large domains (e.g., 10% of the domains have $n_d > 90$ monomers).

Since domains are formed by merging of several rings, they are expected to have a strong internal degree of cross-linking and hence a relatively low deformability. To characterize this feature we calculate the relative fluctuation of the domain size, defined as $\delta = [(\langle R_g^2 \rangle - \langle R_g \rangle^2) / \langle R_g^2 \rangle]^{1/2}$, where R_g is the radius of gyration of the domain, and the brackets denote time average over the simulation trajectory of the domain. Figure 2b shows results of δ for SCNPs *at infinite dilution*, as a function of the number of monomers, n_d , of the domain. Domains with very few monomers ($n_d < 5$) have very closed structures and, as expected, are weakly deformable and show the lowest relative fluctuations. By increasing the domain size, the value of δ increases, until reaching an ultimate plateau for $n_d \gtrsim 50$. The plateau value $\delta_p \sim 0.09$ indicates that even the largest domains have a low relative deformability. It is worthy of remark that, in general, the whole SCNPs have a higher relative deformability than the domains ($\delta_{\text{SCNP}} > \delta_p$ for 85 % of the SCNPs, see ordinate in Figure 2d below). These observations justify the introduction of domains as defined above to characterize relatively compact, weakly deformable regions of the SCNPs, which can be seen as counterparts of the domains in IDPs. Moreover, the above defined domains allow to

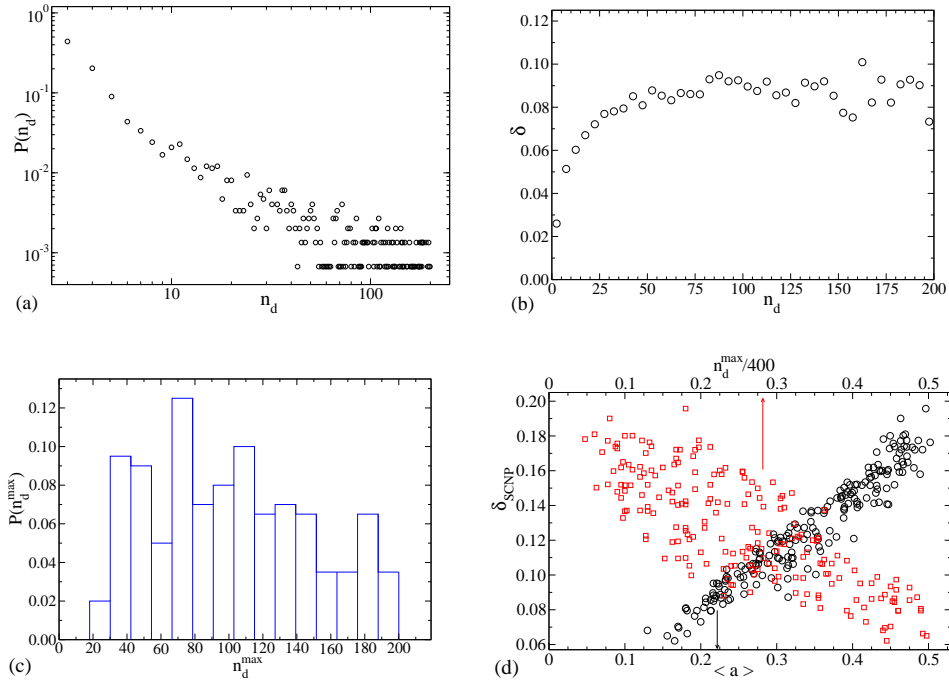


Figure 2: (a): Distribution of the domain size n_d . (b): Relative fluctuation δ (see text) of the domain vs. its number of monomers n_d , at infinite dilution. To improve the statistics, we average δ over intervals $n_0 < n_d \leq n_1$, where n_0, n_1 are consecutive multiples of 5. (c): Distribution of n_d^{\max} . (d): Relative fluctuation δ_{SCNP} , at infinite dilution, of the SCNP vs. its asphericity $\langle a \rangle$ (circles, bottom axis) and size of the maximum domain n_d^{\max} (squares, top axis). Data for n_d^{\max} are normalized by 400, providing a common abscissa for a fair comparison of the dispersion of both data sets.

introduce a structural/geometrical characterization of internal disorder in SCNPs. We note that, in the case of IDPs, quantification of disorder is usually based on chemical criteria correlated with the formation of secondary structure (e.g., the charge-hydrophathy plot²¹). Still, the need of specific structural or geometrical parameters to characterize internal disorder in nano-objects like SCNPs or IDPs seems imperative to look for correlations between disorder and functionality. On this basis, a meaningful parameter to identify internal disorder in a SCNP can be given by the size of its largest domain (defined by the number of monomers, n_d^{\max} , in that domain). Thus, SCNPs with low n_d^{\max} can be considered more disordered than those with high n_d^{\max} . Figure 2c shows the distribution of n_d^{\max} . A very broad distribution is found, extending from $n_d^{\max} \sim 20$ to the maximum size $n_d^{\max} = N = 200$. This demonstrates

that SCNPs, in analogy with IDPs, can exhibit architectures with very different degree of disorder, being formed by the connection of several small domains, by a single big domain, or by combinations of small and big domains. Figure 2d demonstrates the correlation between internal disorder and relative deformability δ_{SCNP} of the SCNP (see squares). This is also an indication of the correlation between disorder and functionality, since indeed δ_{SCNP} reflects internal mobility — a relevant parameter in the context of potential functionality.

We also introduce a geometrical parameter, the asphericity a , that can be related to the degree of disorder of the SCNP. This is calculated as³⁴ $a = (1/2)[(I_2 - I_1)^2 + (I_3 - I_1)^2 + (I_3 - I_2)^2]/[I_1 + I_2 + I_3]^2$, where I_1, I_2, I_3 are the eigenvalues of the radius of gyration tensor of the macromolecule. Because of the topological polydispersity, each individual SCNP has a different asphericity $\langle a \rangle$, where brackets denote time-average over the trajectory of the SCNP. The asphericity is a strong predictor of the internal mobility of the SCNP. This is demonstrated in Figure 2d (circles), which shows the strong correlation between the fluctuation δ_{SCNP} of the whole SCNP at $\rho \rightarrow 0$ and the asphericity. In what follows we will discuss the conformational properties of SCNPs as a function of their degree of disorder. After the discussion above, we will use the size of the maximum domain, $n_{\text{d}}^{\text{max}}$, to discriminate the most disordered SCNPs (lowest $n_{\text{d}}^{\text{max}}$). We will use instead the asphericity $\langle a \rangle$ to discern the most ordered SCNPs (lowest $\langle a \rangle$). Indeed $\langle a \rangle$ is better correlated than $n_{\text{d}}^{\text{max}}$ with low deformability (Figure 2d), providing a highly discriminative characterization of order in terms of functionality.

Now we investigate crowding effects on concentrated solutions of SCNPs, by analyzing the density dependence of their conformational properties. Because of the observed topological polydispersity, each SCNP may be expected to show a different collapse behavior under crowding conditions. This is confirmed in Figure 3a, which shows the compression ratio of the radius of gyration, $r = (\langle R_{\text{g}}^2 \rangle / \langle R_{\text{g}0}^2 \rangle)^{1/2}$, with increasing density ρ , where $R_{\text{g}0}$ is the radius of gyration at infinite dilution. Results are given for the average over all the SCNPs, as well as for the 10 % most ordered and most disordered SCNPs (according, respectively,

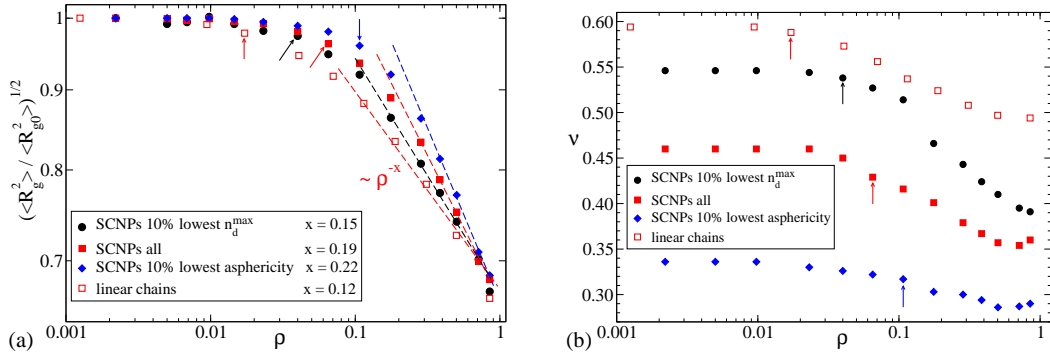


Figure 3: (a): Reduction of the radius of gyration with increasing density. Different data sets (see legend) show results averaged for all the SCNPs, and for the 10 % of SCNPs with the lowest asphericity (most ordered SCNPs) and the lowest n_d^{\max} (most disordered SCNPs). For comparison, we include data for the linear precursors. Dashed lines are fits to power-laws $\sim \rho^{-x}$. The values of x are given in the legend. (b): For the same groups of macromolecules of (a), density dependence of the scaling exponent ν of the form factor in the fractal regime. Arrows in both panels indicate the overlap density ρ^* .

to their values of asphericity and n_d^{\max}). For comparison we include the results for the solutions of the linear precursors. By increasing concentration there is a sharp crossover from almost ρ -independent behavior to power-law behavior. The crossover occurs at the overlap density (indicated by arrows in Figure 3). The latter is defined as $\rho^* = N \langle D_{g0}^2 \rangle^{-3/2}$, with D_{g0} the diameter of gyration at $\rho \rightarrow 0$, and corresponds to the density for the onset of intermolecular contacts at all the macromolecular peripheria. The power-laws $r \sim \rho^{-x}$ observed in Figure 3a for $\rho > \rho^*$ are characterized by different exponents, varying from the well-known value $x \approx 0.12$ for the linear chains^{16,32} to $x \approx 0.22$ for the 10% most ordered SCNPs.

Insight on the effect of crowding on the average intramolecular structure of the SCNPs can also be obtained by analyzing their form factor as a function of concentration. The form factor is defined as $w(q) = \langle N^{-1} \sum_{j,k} \exp[i\mathbf{q} \cdot (\mathbf{r}_j - \mathbf{r}_k)] \rangle$, where q is the wavevector, $\mathbf{r}_{j,k}$ are monomer positions and the sum is restricted over monomers in the same SCNP. Fig. S1 in the SI displays representative cases of the obtained form factors, showing that crowding does not only lead to a reduction of the size, but also to a change in the shape

of the macromolecule. This becomes evident by inspection of the slope of $w(q)$ in the fractal regime,¹⁶ $\langle R_g^2 \rangle^{-1/2} \lesssim q \lesssim b^{-1}$, where b is the bond length. This range corresponds to $0.2 \lesssim q \lesssim 1$ for the simulated systems. In the fractal regime the form factor scales as $w(q) \sim q^{-1/\nu}$, with ν the scaling exponent.¹⁶ Figure 3b shows the density dependence of ν for the same groups of macromolecules of Figure 3a and S1. Concomitant with the reduction of the macromolecular size with increasing density, there is a decrease of the exponent ν . This is a signature of the collapse to more compact conformations. As expected, the exponent for the linear chains changes from the Flory value ($\nu \approx 0.59$), characteristic of isolated ($\rho \rightarrow 0$) self-avoiding chains in good solvent, to the value $\nu = 1/2$ characteristic of the Gaussian conformations¹⁶ at melt density ($\rho \rightarrow 1$). A different behavior is found for the SCNPs. At $\rho \rightarrow 0$ the average form factor shows an exponent $\nu \approx 0.46$, similar to the *average* value $\nu \sim 0.5$ found for isolated IDPs.¹⁷ By increasing density there is a transition to an ultimate exponent $\nu \approx 0.36$ ($w(q) \sim q^{-2.8}$) at $\rho \gtrsim 0.4$. The observed exponent $\nu \sim 1/3$ is consistent with globular conformations (fractal dimension¹⁶ $D = \nu^{-1} \sim 3$). However these do not correspond to homogeneous compact spheres, which in the range $\langle R_g^2 \rangle^{-1/2} \lesssim q \lesssim b^{-1}$ would be dominated by Porod scattering ($w(q) \sim q^{-4}$) followed by oscillatory behavior.¹⁶ Instead, the observed scaling behavior resembles that characteristic of the *crumpled globular* conformations recently observed in melts of polymer rings.^{31–33} These conformations are characterized by relatively large compact regions surrounded by extended protrusions. As anticipated in Figure 1(c-d), the inspection of snapshots confirm that indeed these are the general conformations of the SCNPs at concentrated solutions. Fig. S2a in the SI shows a portion of the simulation box for a solution of SCNPs at $\rho = 0.3$. It becomes evident that crumpled globular conformations are much more compact and less interpenetrated than the conformations of linear chains at the same density (Fig. S2b in the SI).

Figure 3b includes the density dependence of ν for the 10% most ordered and most disordered SCNPs. The data reveal that very different degrees of internal disorder result in very different scaling exponents for the SCNPs. As anticipated by their low asphericity

values, the most ordered SCNPs are already crumpled globular objects at infinite dilution ($\nu \approx 0.33$). Crowding at high densities changes the exponent to $\nu \approx 0.29$. This is close to the behavior $w(q) \sim q^{-4}$ for homogeneous spheres, though the SCNPs still contain local inhomogeneities and voids (see Figure 1d). In the case of the most disordered SCNPs we find an exponent $\nu \approx 0.55$ at infinite dilution, close to the Flory exponent $\nu = 0.59$ for perfectly linear chains in good solvent. This is consistent with the small size of the domains in the most disordered SCNPs ($n_d^{\max} < 0.2N$ for the selected 10 %). By increasing concentration the exponent changes to an ultimate value $\nu \approx 0.39$, somewhat higher than the average $\nu \approx 0.36$ for SCNPs, but clearly below the value $\nu = 1/2$ expected for melts of linear chains,¹⁶ as well as for melts of *Gaussian* rings (where the ring architecture is kept but the chain uncrossability condition is removed).³¹ In summary, in close analogy with the case of polymer rings, the particular architecture of the SCNPs in combination with the chain uncrossability condition results in very different topological interactions from those of linear chains. As a consequence, linear chains and SCNPs show a very different collapse behavior under macromolecular crowding (collapsing to Gaussian chains and crumpled globules, respectively).

It is worthy of remark that crumpled globular conformations ($\nu \sim 1/3$) for the SCNPs are not only found at melt densities ($\rho \sim 1$). They are generally observed already at concentrations of $\rho \sim 0.3$ (see data averaged over all SCNPs in Figure 3b). Even in the case of the 10% most disordered SCNPs we observe at such concentrations exponents $\nu \sim 0.4$, clearly below that of Gaussian chains ($\nu = 1/2$). Since an occupied volume fraction of about 30% is usual in cellular environments, the results presented here for concentrated solutions of SCNPs potentially provide a general scenario for understanding collapse behavior of IDPs under crowding conditions *in vivo*.

We can provide experimental evidence to the above proposed scenario by means of SANS experiments on real SCNPs. On the one hand, we consider SCNPs in highly diluted solution with a good solvent consisting of small molecules. On the other hand, the SCNPs are dispersed in a bulky matrix of polymeric crowders of comparable dimensions. Exploiting the

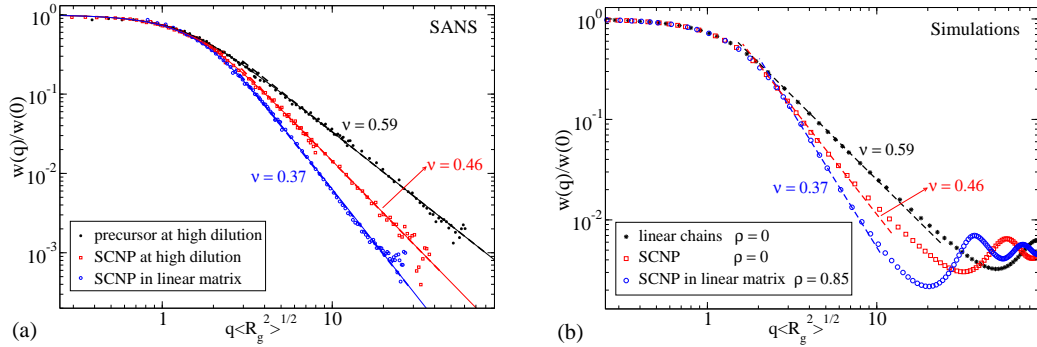


Figure 4: (a): Normalized form factor of real macromolecules in different environments determined by SANS and represented against the reduced variable $q\langle R_g^2 \rangle^{1/2}$: linear precursor chains and the corresponding SCNPs at high dilution, and SCNPs immersed in a linear polymeric matrix. Solid lines are fits to generalized Gaussian coil functions, Eq. (1). Dashed lines are power-law fits, $w(q) \sim q^{-1/\nu}$, in the fractal regime. The scaling exponents ν are indicated. (b): as panel (a) for the simulation results. The first peak at high- q in the simulations ($q \sim 7$ in absolute units) corresponds to the typical bond distance and next peaks are higher harmonics. These local scales are out of the experimental SANS window.

huge difference in the scattering length of the hydrogen and deuterium nuclei, SANS experiments reveal the form factor of the protonated entities on systems where protonated macromolecules are surrounded by a deuterated environment. Protonated SCNPs were obtained through Michael addition-mediated multidirectional self-assembly of individual polymeric chains (precursors) based on methyl methacrylate. The obtained SCNPs were dispersed in a good solvent (deuterated dimethylformamide, dDMF) or in a bulky matrix of deuterated poly(ethylene oxide) (dPEO). The weak (favorable) interaction between the two polymers³⁵ assures thermodynamic miscibility in the SCNP/dPEO system. The molecular weights of dPEO and the SCNPs were very similar (96 and 92 kg/mol, respectively). To measure the form factor (intramolecular correlations) avoiding contributions of the structure factor (all correlations) to the measured signal, the used concentration of SCNPs was very low (2 mg/mL in the solution and 4% in weight in the dPEO matrix). As reference, we also investigated the analogous dilute solution of linear precursors in dDMF. More details about the synthesis, sample preparation and experimental conditions can be found in the SI.

The results for the three samples investigated are presented in Figure 4a. The intensity

has been normalized by its $q \rightarrow 0$ asymptotic value, delivering directly the normalized form factor $w(q)/w(0)$ of the labeled macromolecules in the deuterated environment. Using as abscissa the reduced variable $q\langle R_g^2 \rangle^{1/2}$, the differences in the fractal regime can be clearly appreciated. The slope of the curves strongly increases in dilute solution from the precursor to the SCNP, and from the SCNP in dilute solution to the crowded environment imposed by the PEO-chains. As can be seen in Figure 4a, the data can be well described by generalized Gaussian coil functions³⁶

$$\frac{w(q)}{w(0)} = \frac{1}{\nu U^{\frac{1}{2\nu}}} \gamma\left(\frac{1}{2\nu}, U\right) - \frac{1}{\nu U^{\frac{1}{\nu}}} \gamma\left(\frac{1}{\nu}, U\right) \quad (1)$$

with $U = (2\nu + 1)(2\nu + 2)q^2\langle R_g^2 \rangle/6$ and $\gamma(a, x) = \int_0^x t^{a-1} \exp(-t) dt$. These fits (solid lines in Figure 4a) provide simultaneously the radius of gyration and the scaling exponent ν . Still, the same values of ν are found within the error bars of simple power-law fits $w(q) \sim q^{-1/\nu}$ in the fractal regime (dashed lines). The obtained scaling exponents are $\nu = 0.59$ for the precursors in dilute solution (as expected for self-avoiding linear chains), 0.46 for the SCNPs in dilute solution and 0.37 for the SCNPs in the bulky sample. The compaction revealed by this parameter is accompanied by the concomitant reduction of the macromolecular dimensions, characterized for this molecular weight by radii of gyration of 8.5 nm (precursor in dilute solution), 6.8 nm (SCNPs in dilute solution) and 5.8 nm (SCNPs in bulky environment). Figure 4b shows the corresponding simulation results for the linear chains and SCNPs at $\rho \rightarrow 0$, and for the SCNPs diluted in a mixture with linear chains (at bulk-like total density $\rho = 0.85$). Remarkably, the exponents found in the experiments are in full agreement with the simulations, confirming the collapse scenario proposed for SCNPs under macromolecular crowding.

In summary, we have presented for the first time a global picture for the conformational properties of SCNPs in solution, covering the whole concentration range from infinite dilution to melt density. Our simulation results are confirmed by SANS experiments. By identifying

in the SCNP structure weakly deformable compact regions (domains) connected by flexible segments, we establish a structural analogy with IDPs. Thereby, the generic trends reported here propose a general scenario for the non-specific, purely steric effects of macromolecular crowding on IDPs in cell environments. These effects lead by themselves to the collapse of the IPDs into crumpled globular conformations. Only in the limit of fully disordered linear architectures, IDPs adopt Gaussian conformations under crowding conditions.

Supporting Information

Description of the simulated model, simulation procedure, sample preparation and SANS measurements. Representative form factors (Figure S1) and simulation snapshots in concentrated solutions (Figure S2).

Acknowledgments

We thank I. Asenjo and M. Gonzalez-Burgos for their help with sample preparation and A. Radulescu and J. Kohlbrecher for their assistance during the SANS experiments. Financial support from the Projects MAT2012-31088 and IT-654-13 (GV) is acknowledged. This work is based on experiments performed at SANS-1 (SINQ, Paul Scherrer Institute, Villigen, Switzerland), and KWS-2 (Heinz Maier-Leibnitz Zentrum (MLZ), Garching, Germany), and has been supported by the European Commission under the 7th Framework Programme through the 'Research Infrastructures' action of the 'Capacities' Programme, NMI3-II Grant Number 283883.

References

- (1) Altintas O.; Barner-Kowollik C. Single chain folding of synthetic polymers by covalent and non-covalent interactions: Current status and future perspectives. *Macromol.*

- Rapid. Commun.* **2012**, *33*, 958-971.
- (2) Lyon C. K.; Prasher A.; Hanlon A. M.; Tuten B. T.; Tooley C. A.; Frank P. G.; Berda E. B. A brief user's guide to single-chain nanoparticles. *Polym. Chem.* **2014**, *6*, 181-197.
 - (3) Gonzalez-Burgos M.; Latorre-Sanchez A.; Pomposo J. A. Advances in single chain technology. *Chem. Soc. Rev.* **2015**, *44*, 6122-6142.
 - (4) Mavila S.; Eivgi O.; Berkovich I.; Lemcoff N. G. Intramolecular cross-linking methodologies for the synthesis of polymer nanoparticles. *Chem. Rev.* (ASAP) 10.1021/acs.chemrev.5b00290.
 - (5) Hamilton S. K.; Harth E. Molecular dendritic transporter nanoparticle vectors provide efficient intracellular delivery of peptides. *ACS Nano* **2009**, *3*, 402-410.
 - (6) Sanchez-Sanchez A.; Akbari S.; Moreno A. J.; Lo Verso F.; Arbe A.; Colmenero J.; Pomposo J. A. Design and preparation of single-chain nanocarriers mimicking disordered proteins for combined delivery of dermal bioactive cargos. *Macromol. Rapid. Commun.* **2013**, *34*, 1681-1686.
 - (7) Gillissen M. A. J.; Voets I. K.; Meijer E. W.; Palmans A. R. A. Single chain polymeric nanoparticles as compartmentalised sensors for metal ions. *Polym. Chem.* **2012**, *3*, 3166-3174.
 - (8) Perez-Baena I.; Loinaz I.; Padro D.; Garcia I.; Grande H. J.; Odriozola I. Single-chain polyacrylic nanoparticles with multiple Gd(III) centres as potential MRI contrast agents. *J. Mater. Chem.* **2010**, *20*, 6916-6922.
 - (9) Bai Y.; Xing H.; Vincil G. A.; Lee J.; Henderson E. J.; Lu Y.; Lemcoff N. G.; Zimmerman S. C. Practical synthesis of water-soluble organic nanoparticles with a single reactive group and a functional carrier scaffold. *Chem. Sci.* **2014**, *5*, 2862-2868.

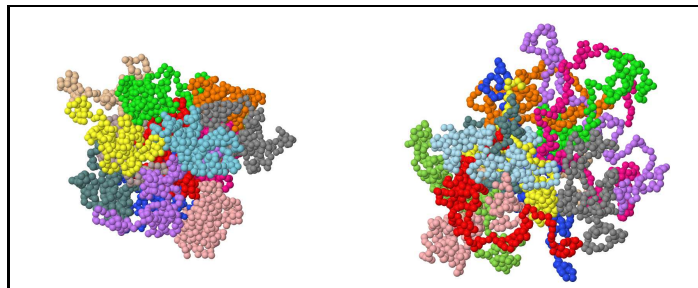
- (10) Terashima T.; Mes T.; De Greef T. F. A.; Gillissen M. A. J.; Besenius P.; Palmans A. R. A.; Meijer E. W. Single-chain folding of polymers for catalytic systems in water. *J. Am. Chem. Soc.* **2011**, *133*, 4742-4745.
- (11) Perez-Baena I.; Barroso-Bujans F.; Gasser U.; Arbe A.; Moreno A. J.; Colmenero J.; Pomposo, J. A. Endowing single-chain polymer nanoparticles with enzyme-mimetic activity. *ACS Macro. Lett.* **2013**, *2*, 775-779.
- (12) Huerta E.; Stals P. J. M.; Meijer E. W.; Palmans A. R. A. Consequences of folding a water-soluble polymer around an organocatalyst. *Angew. Chem. Int. Ed.* **2013**, *52*, 2906-2910.
- (13) Sanchez-Sanchez A.; Akbari S.; Etxeberria A.; Arbe A.; Gasser U.; Moreno A. J.; Colmenero J.; Pomposo J. A. 'Michael' nanocarriers mimicking transient-binding disordered proteins. *ACS Macro Lett.* **2013**, *2*, 491-495.
- (14) Moreno A. J.; Lo Verso F.; Sanchez-Sanchez A.; Arbe A.; Colmenero J.; Pomposo J. A. Advantages of orthogonal folding of single polymer chains to soft nanoparticles. *Macromolecules* **2013**, *46*, 9748-9759.
- (15) Pomposo J. A.; Pérez-Baena I.; Lo Verso F.; Moreno A. J.; Arbe A.; Colmenero J. How far are single-chain polymer nanoparticles in solution from the globular state?. *ACS Macro Lett.* **2014**, *3*, 767-772.
- (16) Rubinstein M.; Colby R. H. *Polymer Physics*; Oxford University Press: Oxford, UK, 2003.
- (17) Marsh J. A.; Forman-Kay J. D. Sequence determinants of compaction in intrinsically disordered proteins. *Biophys. J.* **2010**, *98*, 2383-2390.
- (18) Hofmann H.; Soranno A.; Borgia A.; Gast K.; Nettels D.; Schuler B. Polymer scaling

- laws of unfolded and intrinsically disordered proteins quantified with single-molecule spectroscopy. *Proc. Natl. Acad. Sci. USA* **2012**, *109*, 16155-16160.
- (19) Bernadó P.; Svergun D. I. Structural analysis of intrinsically disordered proteins by small-angle X-ray scattering. *Mol. BioSyst.* **2012**, *8*, 151-167.
- (20) Receveur-Brechot V.; Durand D. How random are intrinsically disordered proteins? a small angle scattering perspective. *Curr. Protein Pept. Sci.* **2012**, *13*, 55-75.
- (21) Habchi J.; Tompa P.; Longhi S.; Uversky V. N. Introducing protein intrinsic disorder. *Chem. Rev.* **2014**, *114*, 6561-6588.
- (22) Van der Lee R.; Buljan M.; Lang B.; Weatheritt R. J.; Daughdrill G. W.; Dunker A. K.; Fuxreiter M.; Gough J.; Gsponer J.; Jones D. T.; Kim P. M.; Kriwacki R. W.; Oldfield C. J.; Pappu R. V.; Tompa P.; Uversky V. N.; Wright P. E.; Babu M. M. Classification of intrinsically disordered regions and proteins. *Chem. Rev.* **2014**, *114*, 6589-6631.
- (23) Theillet F. X.; Binolfi A.; Fremdgen-Kesner T.; Hingorani K.; Sarkar M.; Kyne C.; Conggang L.; Crowley P. B.; Gierasch L.; Pielak G. J.; Elcock A. H.; Gershenson A.; Selenko P. Physicochemical properties of cells and their effects on intrinsically disordered proteins (IDPs). *Chem. Rev.* **2014**, *114*, 6661-6714.
- (24) Zhou H. X.; Rivas G.; Minton A. P. Macromolecular crowding and confinement: biochemical, biophysical, and potential physiological consequences. *Annu. Rev. Biophys.* **2008**, *37*, 375-379.
- (25) Soranno A.; Koenig I.; Borgia M. B.; Hofmann H.; Zosel F.; Nettels D.; Schuler B. Single-molecule spectroscopy reveals polymer effects of disordered proteins in crowded environments. *Proc. Natl. Acad. Sci. USA* **2014**, *111*, 4874-4879.
- (26) Johansen D.; Jeffries C. M. J.; Hammouda B.; Trewhella J.; Goldenberg D. P. Effects of

- macromolecular crowding on an intrinsically disordered protein characterized by small-angle neutron scattering with contrast matching. *Biophys. J.* **2011**, *100*, 1120-1128.
- (27) Le Coeur C.; Demé B.; Longeville S. Compression of random coils due to macromolecular crowding. *Phys. Rev. E* **2009**, *79*, 031910.
- (28) Le Coeur C.; Teixeira J.; Busch P.; Longeville S. Compression of random coils due to macromolecular crowding: Scaling effects. *Phys. Rev. E* **2010**, *81*, 061914.
- (29) Qin S.; Zhou H. X. Effects of macromolecular crowding on the conformational ensembles of disordered proteins. *J. Phys. Chem. Lett.* **2013**, *4*, 3429-3434.
- (30) Kang H.; Pincus P. A.; Hyeon C.; Thirumalai D. Effects of macromolecular crowding on the collapse of biopolymers. *Phys. Rev. Lett.* **2015**, *114*, 068303.
- (31) Halverson J. D.; Lee W. B.; Grest G. S.; Grosberg A. Y.; Kremer K. Molecular dynamics simulation study of nonconcatenated ring polymers in a melt. I. Statics. *J. Chem. Phys.* **2011**, *134*, 204904.
- (32) Reigh S. Y.; Yoon D. Y. Concentration dependence of ring polymer conformations from Monte Carlo simulations. *ACS Macro Lett.* **2013**, *2*, 296-300.
- (33) Goossen S.; Bras A. R.; Krutyeva M.; Sharp M.; Falus P.; Feoktystov A.; Gasser U.; Pyckhout-Hintzen W.; Wischnewski A.; Richter D. Molecular Scale Dynamics of Large Ring Polymers. *Phys. Rev. Lett.* **2014**, *113*, 168302.
- (34) Rawdon E. J.; Kern J. C.; Piatek M.; Plunkett P.; Stasiak A.; Millett K. C. Effect of knotting on the shape of polymers. *Macromolecules* **2008**, *41*, 8281-8287.
- (35) Hopkinson I.; Kiff F. T.; Richards R. W.; King S. M.; Farren T. Isotopic labelling and composition dependence of interaction parameters in polyethylene oxide/polymethyl methacrylate blends. *Polymer* **1995**, *36*, 3523-3531.

- (36) Hammouda B.; Small-Angle scattering from branched polymers. *Macromol. Theory Simul.* **2012**, *21*, 372-381.

Graphical TOC Entry



Concentrated solutions of single-chain nanoparticles (left) and linear chains (right).